Acta Oncologica 26 (1987) Fasc. 1

FROM THE DIVISION OF MEDICAL COMPUTER PHYSICS, UPPSALA DATACENTRAL, S-75002 UPPSALA, SWEDEN, DEPARTAMENTO DE RADIOLOGIA, SECCION DE FISICA, HOSPITAL CLINICO UNIVERSITARIO, ZARAGOZA 9, SPAIN AND DEPARTMENT OF RADIATION PHYSICS, KAROLINSKA INSTITUTET AND UNIVERSITY OF STOCKHOLM, S-10401 STOCKHOLM, SWEDEN.

CALCULATION AND APPLICATION OF POINT SPREAD FUNCTIONS FOR TREATMENT PLANNING WITH HIGH ENERGY PHOTON BEAMS

A. AHNESJÖ, P. ANDREO and A. BRAHME

Abstract

A general dose calculation method for treatment planning with high energy photon beams, based on folding of the total energy released by primary photons per unit mass, the terma, with a fractional mean energy imparted point spread function is described. A set of point spread functions has been calculated with Monte Carlo technique for energies of primary photons between 100 keV and 20 MeV. Dose distributions have been calculated for a 6 MV beam using the method. The results clearly point out the considerably increased precision and flexibility achieved when calculating photon beam dose distributions from first principles using Monte Carlo generated point spread functions. The point spread functions calculated in this work are available on magnetic tape from the authors.

Key words: Dosimetry; treatment planning, high energy photons, point spread functions.

In radiation therapy, accurate dose planning is of fundamental importance. The increased availability of computed tomography and to some extent also magnetic resonance imaging for dose plannings has during the last decade made it meaningful to develop accurate 3D dose computation models. The models employed in most present photon dose planning systems are based on the concept of separating the absorbed dose into two components, 'primary' and 'scattered' dose. This concept is valid provided the lepton range (electron and positron range) is less than the desired spatial resolution of the computed dose distribution. However, the range of the leptons released by high energy photons does often exceed the limits given by the demand of resolution for radiotherapy. This, together with difficulties to satisfactory account for arbitrary field shapes, body contours, etc., by present models, increases the need of more general models.

Recently a number of authors has proposed photon dose planning models where both the leptons and scattered photons can be accurately taken into account by means of scattering kernels (1, 12, 13, 17, 21, 22, 25). Many of these authors are also utilizing fast Fourier transform techniques to increase computational speed (1, 12, 13, 21, 22). A convolution model for photons, based on Gaussian kernels, has also been proposed (34, 35). Conceptually, the authors above calculate the absorbed dose distribution by integrating *all* energy components scattered from the site of the primary photon interaction. A related method using Monte Carlo generated photon pencil beams for ^{60}Co has also been described (31).

Assuming an infinite homogeneous medium, it is obvious that the pattern of energy spread around a point of primary interaction is spatially invariant and once calculated it can be used at any point throughout the medium. By disregarding phantom boundary effects, the same energy spread pattern can be applied to finite uniform phantoms of arbitrary shape. In this approximation the integration can, from a mathematical point of view, be described as a convolution of the distribution of total energy released by primary photon interactions per unit mass, here given the name *terma* (analogous to the kerma, the kinetic energy released per unit mass), with a point spread function (PSF) describing the spatial spread of energy from each interaction point.

A crucial step of the proposed method is to determine the point spread functions of different photon beams. Once accurately calculated, they can be used for studying practically all photon beam properties, such as depth dose

Accepted for publication 23 September 1986.

curves, lateral profiles, absence of electron equilibrium near field edges, and so on.

This paper describes the calculation and some applications of absorbed dose point spread functions in water for monoenergetic photon energies, between 100 keV and 20 MeV. The Monte Carlo method is employed in these calculations, where the main interactions of primary and scattered photons and concomitant leptons are fully accounted for. The Monte Carlo method does not present the mathematic difficulties and limitations that the analytic calculations do and the ease of handling boundaries makes this technique particularly useful.

The presently applied Monte Carlo code follows the transport of photons and leptons as an electromagnetic cascade where the principal interactions of primary particles and successive generations of secondary particles are accounted for. The cascade can be initiated by monoenergetic photons or electrons, a given bremsstrahlung or electron energy spectrum or a mixture of the two.

The program was originally developed for studying in detail the physics of the penetration of electron beams in water (2, 3, 6) and has been extensively applied to treatment planning with electron beams (15, 20) and to the calculation of physical quantities in electron and photon beam dosimetry (5, 7, 8, 9, 10, 14).

The entity terma and the point spread function

When a photon beam is impinging on a homogeneous medium the terma is a quantity of fundamental importance. The total energy released by primary photon interactions per unit mass, or the terma, $T(\mathbf{r})$, at a point, $\mathbf{r}$, can be calculated from first principles by taking the divergence of the vectorial energy fluence $\Psi(\mathbf{r})$ of primary photons (33):

$$T(\mathbf{r}) = -\frac{1}{\varrho(\mathbf{r})} \operatorname{div} \Psi(\mathbf{r}) \tag{1}$$

where $\varrho(\mathbf{r})$ is the density distribution of the medium.

By definition the vectorial energy fluence is obtained from the fluence differential in energy and angle (cf. 18):

$$\Psi(\mathbf{r}) = \int\int \Omega E \Phi_{E,\Omega}(\mathbf{r})\, dE d\Omega = \int\int \Omega \Psi_{E,\Omega}(\mathbf{r})\, dE d\Omega \tag{2}$$

After insertion in eq. (1) the total energy released by primary photons per unit mass may be written

$$T(\mathbf{r}) = -\frac{1}{\varrho(\mathbf{r})} \int\int \Omega \cdot \operatorname{grad} \Psi_{E,\Omega}\, dE d\Omega \tag{3}$$

since $\operatorname{div} \Omega$ by definition is equal to zero as Ω is an independent variable.

Since the energy fluence of primary photons from a point source changes most rapidly in the direction of motion Ω of the primary photons the scalar product in eq. (3) is reduced to:

$$T(\mathbf{r}) = -\frac{1}{\varrho(\mathbf{r})} \int \frac{d\Psi_E}{dl} dE \tag{4}$$

where l is the path length in the direction of motion of the primaries. The terma differental in energy, $T_E(\mathbf{r})$ (the situation for a monoenergetic photon beam), is thus given by:

$$T_E(\mathbf{r}) = -\frac{1}{\varrho(\mathbf{r})} \frac{d\Psi_E}{dl} = \frac{\mu}{\varrho}(E, \mathbf{r})\, E \Phi_E(\mathbf{r}) \tag{5}$$

where $\mu/\varrho(E, \mathbf{r})$ is the mass attenuation coefficient of the primary photons of energy E at a point $\mathbf{r}$, and $\Phi_E(\mathbf{r})$ is the primary photon fluence differential in energy at $\mathbf{r}$. For a spectrum of primary photons the terma becomes:

$$T(\mathbf{r}) = \int \frac{\mu}{\varrho}(E, \mathbf{r}) E \Phi_E(\mathbf{r}) dE \tag{5a}$$

To calculate the terma for dose planning purposes, the fluence is given by

$$\Phi_E(\mathbf{r}) = \Phi_E(\mathbf{r}_0) \left(\frac{r_0}{r}\right)^2 e^{-\int_{r_0}^{r} \frac{\mu}{\varrho}(E, \mathbf{l}) \varrho(\mathbf{l})\, dl} \tag{6}$$

where $\Phi_E(\mathbf{r}_0)$ is the primary photon fluence at a point $\mathbf{r}_0$ on a reference surface in front of the patient and the exponential function expresses the mean attenuation along the direction of motion of the primaries $\mathbf{l} = \mathbf{r} - \mathbf{r}_0$ to a point $\mathbf{r}$ in the patient. The mass attenuation coefficient $\mu/\varrho(E, \mathbf{r})$ and the gravimetric density $\varrho(\mathbf{l})$ have to be estimated from CT numbers, possibly by means of tables.

From the terma distribution function the resultant absorbed dose distribution can be obtained if the energy transport of the secondary particles around each interaction point is known. For this purpose the point spread function $h(\mathbf{r})$ is necessary to describe the energy transport by all possible secondary particles, such as single and multiple scattered photons, photoelectric electrons, Compton electrons, electron-positron pairs and all generations of bremsstrahlung photons, Auger electrons, photonuclear particles, and so on. The point spread function $h(\mathbf{r})$ is here defined as the quotient $d\bar{\varepsilon}(\mathbf{r})/E$ by d^3r, where $d\bar{\varepsilon}(\mathbf{r})/E$ is the fractional mean energy imparted in a small volume d^3r at $\mathbf{r}$ when a primary particle of energy E (excluding rest energies) interacts at the origin, i.e.

$$h(\mathbf{r}) = \frac{d\bar{\varepsilon}(\mathbf{r})}{E d^3 r} \tag{7}$$

From energy conservation (rest mass energy changes are here presumed to be negligible) follows that the normalization of the point spread function is such that:

$$\int\int\int_{-\infty}^{\infty} h(\mathbf{r})\, d^3 r \equiv 1 \tag{7a}$$

With this definition the dimension of the point spread function is volume^{-1}. A PSF calculated for a homogeneous medium of density ϱ_0, h_{ϱ_0} can, in the first approximation, be rescaled and used for another homogeneous medium with the same atomic number but of a different density ϱ,h_ϱ. Neglecting density effect difference on the cross-sections (existing e.g. for the collision stopping power of the electrons), the scaling law becomes:

$$h_\varrho(\mathbf{r}) = \left(\frac{\varrho}{\varrho_0}\right)^3 h_{\varrho_0}\left(\frac{\varrho}{\varrho_0}\mathbf{r}\right) \tag{8}$$

Eq. (8) can be generalized to account for inhomogeneous media in an approximate way by introducing the relative mean density along the line from the interaction site at the origin to the deposition site at $\mathbf{r}$ by a spatially dependent scaling factor

$$c(\mathbf{r}) = \frac{1}{\varrho_0}\int_0^1 \varrho(\alpha\mathbf{r})\,\mathrm{d}\alpha \tag{9}$$

where α is a dimension less linear scale ranging from 0 to 1. Using eq. (9), the generalization of eq. (8) follows:

$$h(\mathbf{r}) \approx \frac{\varrho(\mathbf{r})}{\varrho_0} c^2(\mathbf{r})\, h_{\varrho_0}(c(\mathbf{r})\,\mathbf{r}) \tag{10}$$

which is exactly valid only for dose contributions from particles scattered rectilinear from the origin, i.e. for the first scatter kerma. The PSF at energy E and density ϱ_0, $h_{\varrho_0}(E,\mathbf{r})$, can be calculated by using a Monte Carlo code, forcing the primary photons to interact at the center of a large water phantom.

Provided the terma differential in energy, $T_E(\mathbf{r})$, and the PSF $h_{\varrho_0}(E,\mathbf{r})$ for a medium of density ϱ_0 and energy E are known and neglecting the obliquity of the central axis of the point spread functions due to geometric divergence of the primary photon field, the absorbed dose can be calculated from

$$D(\mathbf{r}) = \int\int\int\int T_E(\mathbf{s})\, h_{\varrho_0}(E,\mathbf{r}-\mathbf{s})\,\mathrm{d}^3s\,\mathrm{d}E \tag{11}$$

where $\mathbf{r}$ is the field point and $\mathbf{s}$ the source points of the energy imparted to $\mathbf{r}$. With use of eq. (8), eq. (11) can be generalized for a homogeneous medium of arbitrary density ϱ

$$D(\mathbf{r}) = \int\int\int\int T_E(\mathbf{s})\left(\frac{\varrho}{\varrho_0}\right)^3 h_{\varrho_0}\left(E,\frac{\varrho}{\varrho_0}(\mathbf{r}-\mathbf{s})\right)\mathrm{d}^3s\,\mathrm{d}E \tag{12}$$

which also is consistent with the theorem of O'Connor (29, 30). The spatial integral in eq. (11, 12) is a 3D convolution and therefore fast Fourier transform techniques can be applied for computational efficiency (1, 12, 13, 21, 22).

For the most general case with a non-uniform medium the absorbed dose distribution may be approximated by

$$D(\mathbf{r}) = \int\int\int\int T_E(\mathbf{s})\frac{\varrho(\mathbf{s})}{\varrho_0} c^2(\mathbf{r},\mathbf{s})\, h_{\varrho_0}(E,c(\mathbf{r},\mathbf{s})(\mathbf{r}-\mathbf{s}))\mathrm{d}^3s\,\mathrm{d}E \tag{13}$$

where the inhomogeneity scaling factor is derived from eq. (9):

$$c(\mathbf{r},\mathbf{s}) = \frac{1}{\varrho_0}\int_0^1 \varrho(\mathbf{r}+\alpha(\mathbf{s}-\mathbf{r}))\,\mathrm{d}\alpha \tag{14}$$

As h in eq. (13) is spatially variant, it is not possible in this general case to use transform techniques to reduce the computation time.

The Monte Carlo code

The Monte Carlo code uses a direct simulation of the photon interactions by considering individual photoelectric absorption, Compton scattering (at all events assuming unpolarized photons) and pair production interactions. Coherent scattering and photonuclear processes are not considered. The electron transport is simulated by dividing the electron tracks into many small segments within which angular deflections and energy losses are small and can be grouped and described by multiple collision models. Large deflections and energy losses are considered individually by direct simulation at the end of each step.

The transport of photons is followed until their energy falls below the Monte Carlo photon cut-off energy, where the energy is locally deposited or the photon interacts outside the phantom, in which case the energy is scored separately for energy balance purposes. Normal values of the photon cut-off energy are between 10 kev and 50 kev for primary photon energies in the range 100 kev to 50 MeV. Energy, position and directional parameters of the generated electrons and positrons are scored separately and followed after the history of primary and scattered photons has been completed.

The grouping of electron interactions mentioned above corresponds to a Class II scheme of mixed procedure (cf. 11). It has been modified by Andreo & Brahme (7) to account for the influence of the parameters governing the classification of interactions in a consistent way.

The classification in large and small events is done with two cut-off parameters, Δ and δ, which limit the maximum energy loss and angular deflection that will be described by a multiple collision theory: continuous slowing down approximation (c.s.d.a.) and multiple scattering approximation for energy losses and angular deflections respectively. Changes greater than Δ and δ are considered individually in a similar manner as for photon interactions, i.e. by direct sampling from the cross section for delta ray production (28) and nuclear scattering (23, 32) respectively. Bremsstrahlung interactions are considered by using the Koch & Motz (19) cross section package.

The two parameters Δ and δ require special attention as theories accounting for restrictions in energy losses and

angular deviations are needed. The well-known restricted stopping power formula accounts for energy losses less than a given cut-off Δ. Energy straggling is already considered in mixed procedures by direct sampling of energy losses between Δ and half the maximum energy of the incident electron from the Möller cross section. Straggling between 0 and Δ can be considered with the use of a restricted straggling theory (cf. 7). Depending on the magnitude of Δ, the neglection of straggling in energy losses less than Δ makes the simulation equivalent to the use of a simple c.s.d.a. model. As discussed previously (cf. 4, 7) this treatment of energy loss-straggling produces better agreement to experimentally determined electron depth dose distributions than that using the theory of LANDAU-BLUNCK-LEISEGANG that predicts a smaller average energy loss than the stopping power theory.

Multiple scattering theories restricted in the maximum deviation angle are needed in order to describe scattering through angles greater than δ in a consistent way. An expression for the restricted mean angle (i.e. a restricted scattering power) has been given by ANDREO & BRAHME (7). The use of two groups to classify angular deviations produces a more accurate treatment of large scattering angles. The large angle scattering events are not properly accounted for with the use of a single Gaussian or a multiple scattering theory such as that due to MOLIÈRE (26, 27).

The transport of leptons is followed until their kinetic energy is lower than the electron cut-off energy, where the energy is locally deposited and two annihilation photons are created in the case of positrons. The cut-off value is governed by the dimensions of the voxel used to compute 3D energy deposition distributions, the corresponding c.s.d.a. range of an electron being less than half of the smaller dimension of the voxel.

To calculate mean energy imparted point spread functions, the first interaction of the primary photons, impinging along the Z axis (Fig. 1), is forced to occur at the origin of the phantom. The imparted energy is scored in voxels of cylindrical geometry, i.e. in cylinders of radius $\Delta r/2$ and thickness Δz on the central axis, and in coaxial rings of radial increment Δr and thickness Δz where the radius is greater than $\Delta r/2$. The origin is chosen to be at the center of the $^1/_2$NZ+1 depth voxel on the central axis where NZ is the number of scoring depths of the phantom. The total scored energy in each voxel is divided by the number of simulated primary photons and their energy to yield the fractional mean energy imparted.

Results and Discussion

By using the present Monte Carlo code a set of 26 point spread functions for water of unit density have been calculated (Table). The number of incident photons in most calculations is 500000 with an approximate CPU-time per run of 80 h on a VAX 750.

Table

Calculated PSFs. The number of bins is 256 radial compartments 512 depth compartments

Primary photon energy MeV	Electron cut-off energy MeV	Size of radial/depth bins Δr cm/Δz cm	Number of primary photons	Fraction of the primary photon energy which is imparted to the scoring geometry
0.1	0.002	0.100/0.100	500 000	0.897
0.2	0.005	0.100/0.100	500 000	0.847
0.3	0.005	0.100/0.100	500 000	0.837
0.4	0.01	0.100/0.100	500 000	0.835
0.4	0.05	0.002/0.002	500 000	0.322
0.5	0.01	0.100/0.100	500 000	0.834
0.6	0.01	0.100/0.100	500 000	0.833
0.7	0.01	0.100/0.100	500 000	0.834
0.8	0.05	0.100/0.100	500 000	0.834
1.0	0.05	0.100/0.100	500 000	0.834
1.0	0.05	0.002/0.002	250 000	0.448
1.25	0.05	0.100/0.100	1 500 000	0.833
1.25	0.05	0.002/0.002	500 000	0.477
1.5	0.15	0.100/0.100	500 000	0.832
2.0	0.10	0.100/0.100	500 000	0.830
2.0	0.05	0.002/0.002	250 000	0.452
2.5	0.10	0.100/0.100	500 000	0.829
3.0	0.15	0.100/0.100	500 000	0.828
3.0	0.05	0.002/0.002	250 000	0.324
4.0	0.15	0.100/0.100	500 000	0.829
4.5	0.15	0.100/0.100	500 000	0.829
5.0	0.15	0.100/0.100	500 000	0.830
6.0	0.15	0.100/0.100	500 000	0.833
10.0	0.15	0.100/0.100	500 000	0.847
15.0	0.15	0.100/0.100	500 000	0.861
20.0	0.15	0.100/0.100	250 000	0.870

In Fig. 1 isolevels of the point spread function $h(\mathbf{r})$ are shown, in units of cm^{-3}, for 0.4, 1.25 and 10.0 MeV primary photons. The number of cascades simulated are 500000, 1500000 and 500000 respectively. These curves very clearly illustrate the change of the scattering pattern with increasing photon energy. We have found that there is a great similarity in isodose patterns for adjacent energies when employing the normalization introduced in equations 7 and 7a. This fact facilitates interpolation between point spread functions calculated at different energies.

The lowest levels located far away from the interaction center are solely due to scattered photons and almost isotropic at the lowest energy, whereas, with increasing photon energy, they become more and more peaked forward. This should be expected from the energy dependence of the cross section for the Compton scattering. The highest isodoses closest to the interaction center, on the other hand, are primarily due to leptons (electrons and positrons) set in motion by the primary photons in photoelectric, Compton and pair producing interaction. The size and shape of this lepton dominated area is determined by the initial angular distribution of electrons and posi-

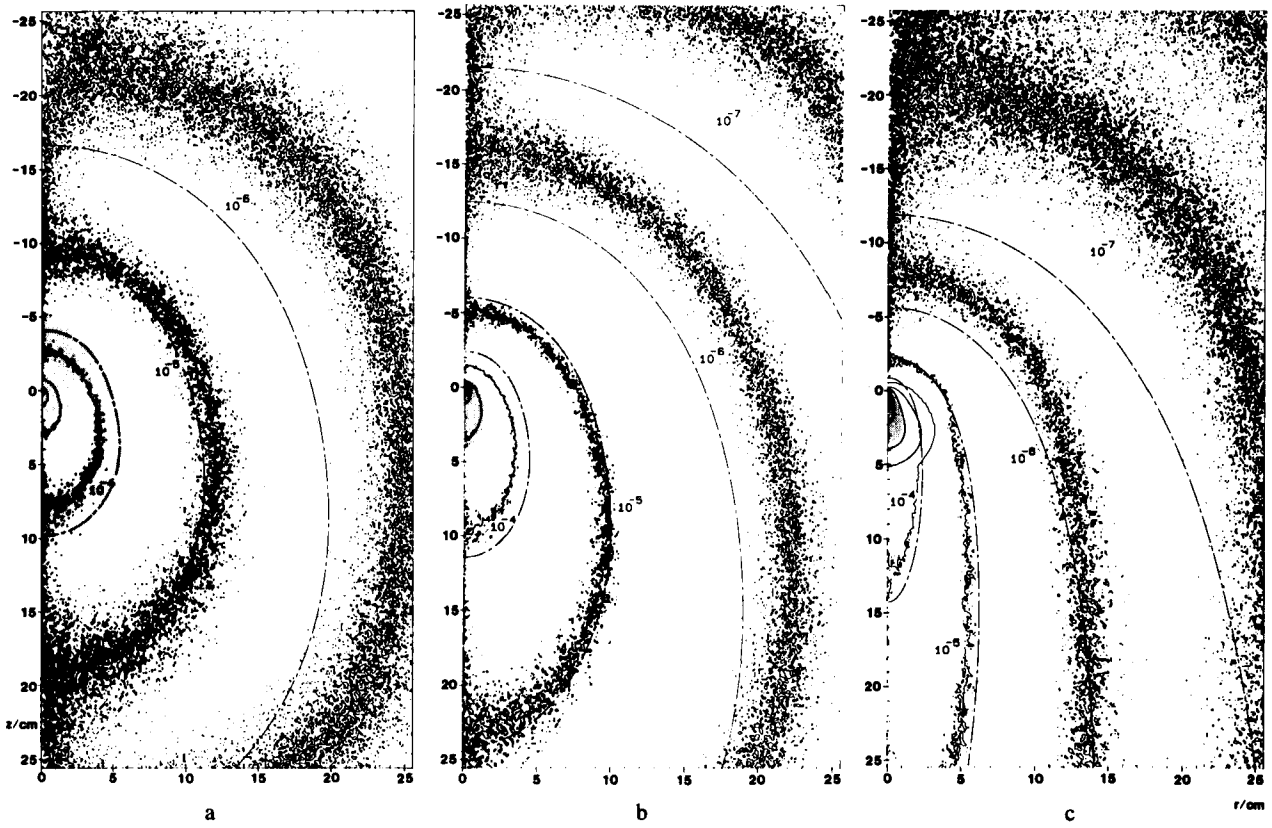

Fig. 1. Isolevels of the point spread function $h(\mathbf{r})$, i.e. the fractional mean energy imparted per unit volume (cm^{-3}), calculated for monoenergetic photons of a) 0.4, b) 1.25 and c) 10.0 MeV respectively. Calculations were made in a cylindrical geometry with 500000, 1500000 and 500000 photons respectively, impinging along the Z axis (left side of the figures) from above and forced to interact at the origin. The separation of the curves is a factor of 10 with maximum values equal to 385.9, 112.9 and 24.7 cm^{-3} respectively. The dash-dotted line is the corresponding distribution of the fractional first scatter terma, calculated using the Klein-Nishina cross sections and neglecting other process than the Compton interaction. The shaded areas cover the volume within which 50% of the incident energy is imparted.

trons, their multiple scatter and finite range. For higher energies the absorbed dose is in the first approximation totally dominated by the electron transport. This is well illustrated in Fig. 1 by the shaded areas enclosing 50 per cent deposition of impinging energy. In Fig. 1c it is seen that more than 50 per cent of the energy imparted is within the range of the first lepton generation at 10 MeV.

The energy transport by electrons and positrons is shown more clearly in Fig. 2, where the PSF due to primary electrons and positrons only is extracted using the Monte Carlo code. The strong forward peaking of the lepton energy deposition is natural as no Compton electrons are leaving the interaction center in the backward hemisphere. However, due to multiple scattering, forward moving electrons may be back-scattered and also a few electrons and positrons produced by pair production may be directed backward. This probably explains the few long range backward directed tracks.

To better illustrate the relative importance of the different dose components the radial energy impartation profile at 45 degrees from the primary photon direction is shown in Fig. 3. It appears that the scattered photon dose contribution is only a few per cent of the primary lepton dose at distances less than the electron range. Just outside the primary lepton range there is a small region dominated by the kerma of single scattered photons, as shown by the lower dashed line. Outside this region the first scatter kerma is considerably less than the mean energy imparted calculated by the Monte Carlo code, indicating the increasing importance of multiple photon scattering at large distances. A rather good analytic approximation to the mean energy imparted at large distances is the first scatter terma, calculated using the Klein-Nishina cross sections and neglecting other processes than the Compton interaction. However, at very large distances and particulary at wide angles, the mean energy imparted is significantly higher than the first scatter terma curves as seen from the dash-dotted lines in Fig. 1. From an energy conservation point of view it is clear that multiple scattered photons and to some extent lepton generated bremsstrahlung photons dominate in regions where the mean energy imparted is considerably larger than the first scatter terma.

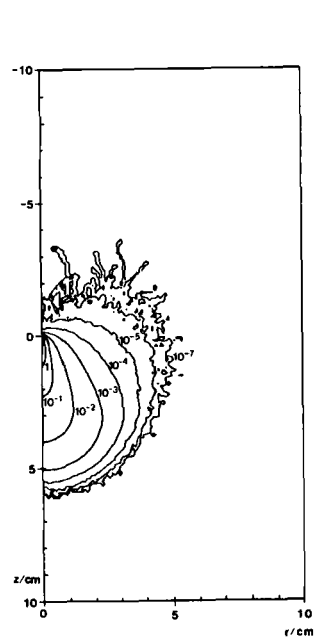

Fig. 2

Fig. 2. Isolevels of the fractional mean energy imparted per unit (cm^{-3}) volume by primary leptons and their secondaries of all generations released by monoenergetic primary photons of 10 MeV at the origin.

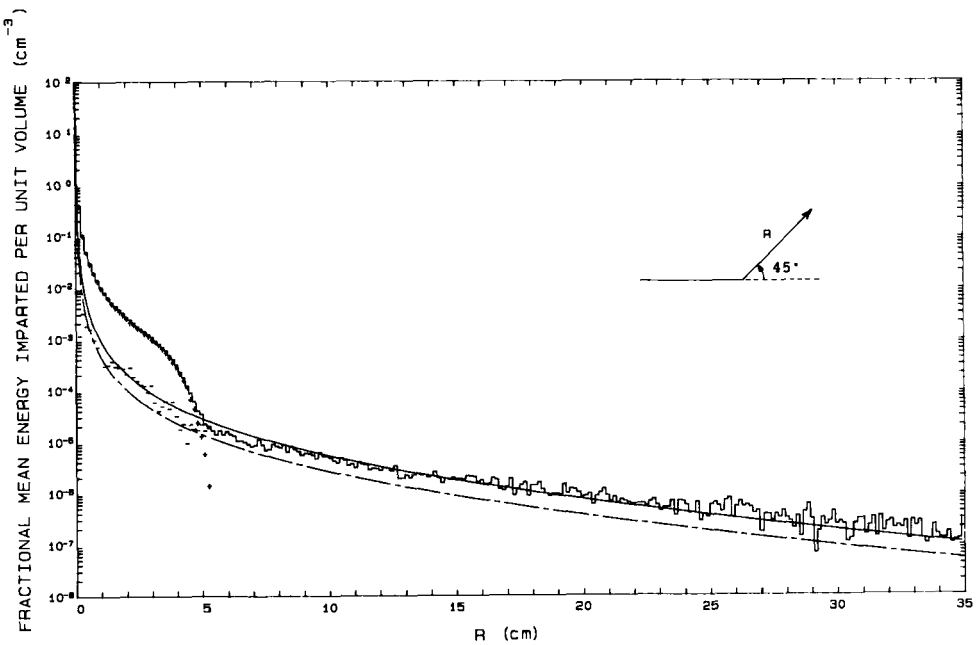

Fig. 3

Fig. 3. Radial plot of the fractional mean energy imparted by primary leptons (+), scattered photon leptons (−) and total energy imparted (solid histogram) at an angle of 45° from the direction of the incident photons. The first scatter terma (−) and first scatter kerma (−·−), analytically calculated using the Klein-Nishina cross sections, are shown.

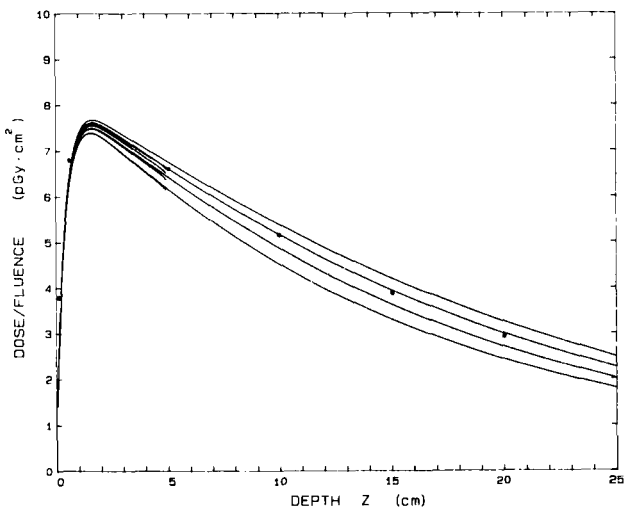

Fig. 4

Fig. 4. Depth dose curves for 6 MV photon beams of 3×3 cm, 6×6 cm, 10×10 cm and 15×15 cm square fields in water phantoms of slab thickness 5 and 25 cm respectively. Experimental data for a 10×10 cm field normalized to the maximum calculated value (●). SSD=100 cm.

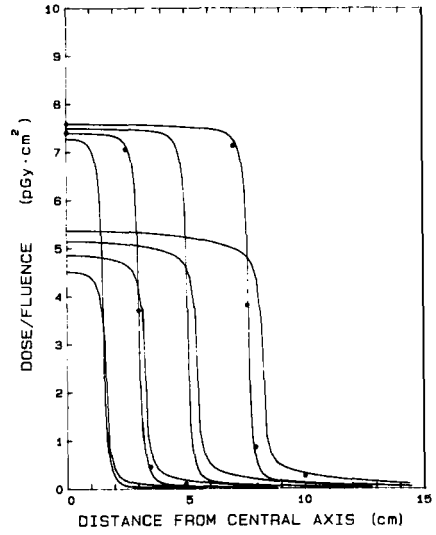

Fig. 5

Fig. 5. 6 MV profiles at 2 and 10 cm depth of 3×3 cm, 6×6 cm, 10×10 cm and 15×15 cm square fields with slab thickness of 25 cm. A point, isotropic source at SSD=100 cm is assumed. Experimental points (●) for the 6×6 cm and 15×15 cm fields normalized on the central axis at each depth.

Central axis depth absorbed dose curves and lateral absorbed dose distributions calculated using equation (11) are shown in Figs 4 and 5. A 6 MV photon spectrum from a medical linear accelerator, published by MOHAN & CHUI (24) was used. The depth dose curves were calculated for a large water phantom but also for a 5 cm thick water slab. 'Infinite' medium PSF were assumed in all cases. The build-up and build-down of the absorbed dose due to the

influence of the lepton transport and the increasing lateral equilibrium of the photon transport with increasing phantom and field size is clearly seen. The substantial influence of the change in the photon back scatter in phantoms of different sizes is clearly seen by comparing the curves for the 5 cm slab with those for the large phantom, particularly at large field sizes.

It is also interesting to note that in pure photon beams the depth of dose maximum is increasing with the field size contrary to the situation in clinical beams where the increasing electron contamination dominates. For comparison experimental data for a 6 MV photon beam (16) are included in the figures.

In Fig. 5 the increased influence of accumulated photon scatter at large depths and field sizes, both inside the beam and outside the penumbra region, is in rather good agreement with experimental data. The deviation outside the field edge noticed in Fig. 6 may partly be explained by the fact that ideal collimators and a point photon source are assumed in the calculations. The depth dose curves and lateral profiles generated by integration of PSF do not show the statistic fluctuations present in the various PSFs because integration is a filtering operation in itself. The integration of approximately 200000 dose components from primary interaction sites in a phantom, each computed using 500000 Monte Carlo histories, is almost equivalent to a Monte Carlo run using 10^{10} histories, needing about 1300 years of VAX 750 CPU-time! This explains the smoothness of all depth dose curves plotted in this work. Such precise results can never be realized by ordinary Monte Carlo calculations due to the large statistic fluctuations in energy deposition by photons.

ACKNOWLEDGEMENTS

This work is supported by the Swedish Medical Research Council (MFR). Use of the computer facilities at the CART demonstrators in Uppsala and Tampere (Finland) has made this work possible. Valuable suggestions from Gudrun Alm-Carlsson, Linköping and comments from Harald Treuer, Heidelberg are gratefully acknowledged.

Request for reprints: Anders Ahnesjö, Division of Medical Computer Physics, Uppsala Datacentral, S-75002 Uppsala, Sweden.

REFERENCES

1. Ahnesjö A.: Application of transform algorithms for calculation of absorbed dose in photon beams. *In*: Computers in radiation therapy, p. 17. Proceedings of the Eighth International Conference on the Use of Computers in Radiation Therapy, Toronto 1984. IEEE Computer Society Press.
2. Andreo P.: Monte Carlo simulation of electron transport in water. Absorbed dose and fluence distributions. Report FANZ/80/3. Dept. of Nuclear Physics, University of Zaragoza, Spain 1980.
3. — Aplicación del Método de Monte Carlo a la penetración y dosimetría de haces de electrones. (In Spanish.) Thesis. University of Zaragoza, Spain 1981.
4. — Monte Carlo simulation of electron transport. Principles and some general results. *In*: The computation of dose distributions in electron beam radiotherapy, p. 80. Edited by A. E. Nahum, University of Umeå, 1985.
5. — and Brahme A.: Mean energy in electron beams. Med. Phys. 8 (1981), 682.
6. — — Fluence and absorbed dose in high energy electron beams. Report RI 1982-05, Department of Radiation Physics, Karolinska Institute, Stockholm (1982). (See also Acta Radiol (1983) Suppl. No. 364, p. 25.)
7. — — Restricted energy loss straggling and multiple scattering of electrons in mixed Monte Carlo procedures. Radiat. Res. 100 (1984), 16.
8. — — Stopping power data for high energy photon beams. Phys. Med. Biol. 3 (1986), 839.
9. — and Nahum A. E.: Stopping-power ratio for a photon spectrum as a weighted sum of the values for monoenergetic photon beams. Phys. Med. Biol. 30 (1985), 1055.
10. — — Influence of initial energy spread in electron beams on the depth-dose distribution and stopping-power ratios. Proceedings of the XIV ICMBE and VII ICMP, p. 608. Espoo, Finland (1985).
11. Berger M. J.: Monte Carlo calculation of the penetration and diffusion of fast charged particles. *In*: Methods in Computational Physics, Vol. 1, Statistical Physics, p. 135. Edited by B. Alder, S. Fernbach and M. Rotenberg. Academic Press, New York 1963.
12. Boyer A. L. and Mok E. C.: Photon beam modelling using Fourier transform techniques. *In*: Computers in Radiation Therapy, p. 14. Proceedings of the Eighth International Conference on the Use of Computers in Radiation Therapy, Toronto 1984. IEEE Computer Society Press.
13. — — A photon does distribution model employing convolution calculations. Med. Phys. 12 (1985), 169.
14. Brahme A. and Andreo P.: Dosimetry and quality specification of high energy photon beams. Acta Radiol. Oncology 25 (1986), 213.
15. — Lax I. and Andreo P.: Electron beam dose planning using discrete Gaussian beams. Mathematical background. Acta Radiol. Oncology 20 (1981), 147.
16. — and Svensson H.: Radiation beam characteristics of a 22 MeV microtron. Acta Radiol. Oncology 18 (1979), 244.
17. Dean R. D.: A scattering kernel for use in true three-dimensional dose calculations. Med. Phys. 7 (1980), 429.
18. ICRU report 35. Radiation dosimetry: Electron beams with energies between 1 and 50 MeV. Bethesda, MD, USA (1984).
19. Koch H. W. and Motz J. W.: Bremsstrahlung cross-section formulas and related data. Rev. Mod. Phys. 31 (1959), 920.
20. Lax I., Brahme A. and Andreo P.: Electron beam dose planning using Gaussian beams. Improved radial dose profiles. Acta Radiol. (1983) Suppl. No. 364, p. 49.
21. Mackie T. R. and Scrimger J. W.: Computing radiation dose for high energy X-rays using a convolution method. *In*: Computers in Radiation Therapy, p. 36. Proceedings of the Eighth International Conference on the Use of Computers in Radiation Therapy, Toronto 1984. IEEE Computer Society Press.
22. — — and Battista J. J.: A convolution method of calculating dose for 15-MV X-rays. Med. Phys. 12 (1985), 188.
23. McKinley W. A. and Feshback H. F.: The Coulomb scattering of relativistic electrons by nuclei. Phys. Rev. 74 (1948), 1759.
24. Mohan R. and Chui C.-S.: Energy and angular distribution of photons from medical linear accelerators. Med. Phys. 12 (1985), 592.
25. — — and Lidofsky L.: Differential pencil beam dose computation model for photons. Med. Phys. 13 (1986), 64.
26. Molière G.: Theorie der Streuung schneller gelandener Teil-

chen. I. Einzelstreuung am abgeschirmten Coulomb-Feld. Z. Naturforsch. A 2 (1947), 133.
27. — Theorie der Streuung schneller geladener Teilchen. II. Mehrfach- und Vielfachstreuung. Z. Naturforsch. A 3 (1948), 79.
28. Möller C.: Zur Theorie des Durchgangs scheneller Elektronen durch Materie. Ann. Phys. 14 (1932), 531.
29. O'Connor J. E.: The variation of scattered X-rays with density in an irradiated body. Phys. Med. Biol. 1 (1957), 352.
30. — The density scaling theorem applied to lateral electronic equilibrium. Med. Phys. 11 (1984), 678.
31. Schoknecht G.: Die Beschreibung von Strahlenfeldern durch Separierung von Primär- und Streustrahlung. IV. Berechnung von Streuverteilungen für parallele Photonenstrahlenfelder. Strahlentherapie 141 (1971), 326.
32. Spencer L. V.: Theory of electron penetration. Phys. Rev. 98 (1955), 1597.
33. Svensson H. and Brahme A.: Recent advances in electron and photon dosimetry. *In*: Radiation dosimetry Physical and biological aspects, p. 87. Edited by C. Orton Plenum, New York 1986.
34. Ulmer W.: On the application of stochastic partition functions for the computation of lateral profiles and depth doses in radiotherapy. Strahlentherapie 158 (1982), 305.
35. — On the application of stochastic partition functions in radiotherapy. II. Modifications of intensity and depth dose profiles by wedge filters. Strahlentherapie 159 (1983), 559.